The Journal of Chemical Physics

RESEARCH ARTICLE | AUGUST 08 2023

Simulating excited-state complex ensembles: Fluorescence and solvatochromism in amine-arene exciplexes

Abhilash Patra ; Anna I. Krylov ; Shaama Mallikarjun Sharada

J. Chem. Phys. 159, 064101 (2023)
https://doi.org/10.1063/5.0158061

The Journal of Chemical Physics ARTICLE pubs.aip.org/aip/jcp

Simulating excited-state complex ensembles: Fluorescence and solvatochromism in amine-arene exciplexes

Cite as: J. Chem. Phys. 159, 064101 (2023); doi: 10.1063/5.0158061
Submitted: 14 May 2023 • Accepted: 11 July 2023 •
Published Online: 8 August 2023

Abhilash Patra,[1] Anna I. Krylov,[2,a)] and Shaama Mallikarjun Sharada[1,2,b)]

AFFILIATIONS

[1] Mork Family Department of Chemical Engineering and Materials Science, University of Southern California, Los Angeles California 90089, USA
[2] Department of Chemistry, University of Southern California, Los Angeles California 90089, USA

Note: This paper is part of the 2023 JCP Emerging Investigators Special Collection.
[a)] **E-mail:** krylov@usc.edu
[b)] **Author to whom correspondence should be addressed:** ssharada@usc.edu

ABSTRACT

Exciplexes are excited-state complexes formed as a result of partial charge transfer from the donor to the acceptor species when one moiety of the donor–acceptor pair is electronically excited. The arene–amine exciplex formed between oligo-(*p*-phenylene) (OPP) and triethylamine (TEA) is of interest in the catalytic photoreduction of CO_2 because it can compete with complete electron transfer to the OPP catalyst. Therefore, formation of the exciplex can hinder the generation of a radical anion $OPP^{\cdot-}$ necessary for subsequent CO_2 reduction. We report an implementation of a workflow automating quantum-chemistry calculations that generate and characterize an ensemble of structures to represent this exciplex state. We use FireWorks, Pymatgen, and Custodian Python packages for high-throughput ensemble generation. The workflow includes time-dependent density functional theory optimization, verification of excited-state minima, and exciplex characterization with natural transition orbitals, exciton analysis, excited-state Mulliken charges, and energy decomposition analysis. Fluorescence spectra computed for these ensembles using Boltzmann-weighted contributions of each structure agree better with experiment than our previous calculations based on a single representative exciplex structure [Kron *et al.*, J. Phys. Chem. A **126**, 2319–2329 (2022)]. The ensemble description of the exciplex state also reproduces an experimentally observed red shift of the emission spectrum of [OPP-4–TEA]* relative to [OPP-3–TEA]*. The workflow developed here streamlines otherwise labor-intensive calculations that would require significant user involvement and intervention.

INTRODUCTION

We report a high-throughput computational workflow to automate quantum-chemical calculation and characterization of exciplexes. An exciplex is an excited-state molecular complex formed by one ground-state and one electronically excited molecule. An exciplex formed between two identical molecules is called an excimer. A distinguishing feature of exciplexes is that they have much stronger bonding than the respective ground-state complexes.[1] Exciplex formation can be observed from the emergence of a structureless, broad fluorescence peak, which is red-shifted relative to the emission peak of the isolated electronically excited acceptor.[1–3] They are encounter complexes formed when the donor and the acceptor are in close proximity. The stabilization of excimers and exciplexes arises due to exciton-resonance and charge-resonance contributions.[4–6] Due to their asymmetry, in exciplexes, partial charge transfer (CT) from the donor to the acceptor is possible, providing the dominant contribution to the bonding. A complete CT results in the formation of a zwitterionic radical pair, quenching the fluorescence.[7,8] In the context of catalytic photoreduction of CO_2, the desired outcome is a complete CT from a sacrificial donor to an electronically excited photocatalyst, and the formation of exciplexes can lead to the reduced yield of the reaction. Numerous experimental and theoretical studies have investigated the electronic structure and properties of excimers and exciplexes.[5,9–16] Such studies support applications in organic light-emitting diodes (OLEDs) via thermally activated

delayed fluorescence (TADF),[17–21] solar energy harvesting via singlet fission,[22–24] chemo-sensors for anionic and cationic surfactant sensing[25–29] and bio-detectors,[30,31] and photoredox catalysis.[32–34]

Advances in quantum-chemistry methods have facilitated accurate modeling of excited states in isolated molecules and the condensed phase. Excimer and exciplex structures have been computed by geometry optimization on excited-state potential energy surfaces (PESs) using configuration interaction singles (CIS),[35] time-dependent density functional theory (TDDFT),[8,11,14,23,34,36–39] equation-of-motion coupled-cluster method for electronically excited states with singles and doubles (EOM-EE-CCSD),[5,12] complete active space self-consistent field (CASSCF), and the algebraic diagrammatic construction scheme to second-order with resolution of identity and spin-opposite scale [RI-SOS-ADC(2)] methods.[40]

The exciplex state can be related to a single structure—the lowest minimum (with sufficient CT character) on the excited-state PES.[34] However, such a description does not account for the fluxional character of these complexes due to a relatively shallow PESs, which may feature multiple accessible minima. This fluxional character can be described by a distribution of structures obtained from sampling the PES (as we perform in this work) or trajectories computed in molecular dynamics simulations.[10,11,13,14,35,38,41] Importantly, not every minimum on the excited-state PES of a molecular complex can be described as exciplex. A recent perspective by our group[34] outlines various approaches that can be employed to verify whether a particular structure has exciplex character or not. The exciplexes can be identified either by wave-function analysis or their optical properties. The former approach includes natural transition orbitals (NTOs),[42–47] exciton descriptors,[48,49] excited-state energy decomposition analysis (EDA),[50] and excited-state Mulliken charge analysis. The property-based approaches utilize the extent of a red shift in fluorescence spectra relative to the isolated excited state (of acceptor) or solvatochromic shifts computed with non-equilibrium solvation models.[51–54]

Once relevant exciplex structures are obtained, one can compute the respective fluorescence spectra. A rigorous procedure would involve the calculation of vibrational broadening by evaluating Franck–Condon factors.[55–60] More often, however, a simpler approach is employed in which only vertical transitions are considered, and the stick spectra are broadened (using empirical parameters) to account for vibrational, inhomogeneous, and instrumental broadening.[61]

This work is motivated by the results of our previous computational and experimental studies on the exciplex formed between the excited-state oligo(*p*-phenylene) (OPP-n) acceptor and ground-state triethylamine (TEA or Et_3N) donor.[34] Experimental studies have shown that OPP consisting of 3 *para*-linked phenyl groups (OPP-3) is a promising photoredox catalyst for CO_2 reduction. The quenching of the excited singlet state of OPP-3 by the sacrificial electron donor, TEA, produces the $OPP^{\bullet-}$ radical anion that goes on to reduce CO_2.[62–64] In our previous work,[34] exciplex formation by TEA and OPP-3* was confirmed by using fluorescence spectroscopy—i.e., by observing the emission peak whose intensity was decreasing with the increasing solvent dielectric (Fig. 1).[34] The experimental observations were complemented by calculations. Specifically, we employed TDDFT to calculate the structure of the [OPP-3–TEA]* exciplex and verified its partial CT character by using NTOs, excited-state EDA, and Mulliken charge analysis. The results have shown that the calculated solvatochromic shifts span a more narrow range than the experimental shifts. Moreover, the calculations yielded nearly identical emission energies for [OPP-3–TEA]* and [OPP-4–TEA]*, in disagreement with the experimentally observed red-shifted emission of the latter in all examined solvents.

On the basis of these observations and the fact that the exciplexes feature broad emission peaks, we hypothesize that a single structure is not sufficient to describe the exciplex and its emission characteristics. We adopt an ensemble approach in which several

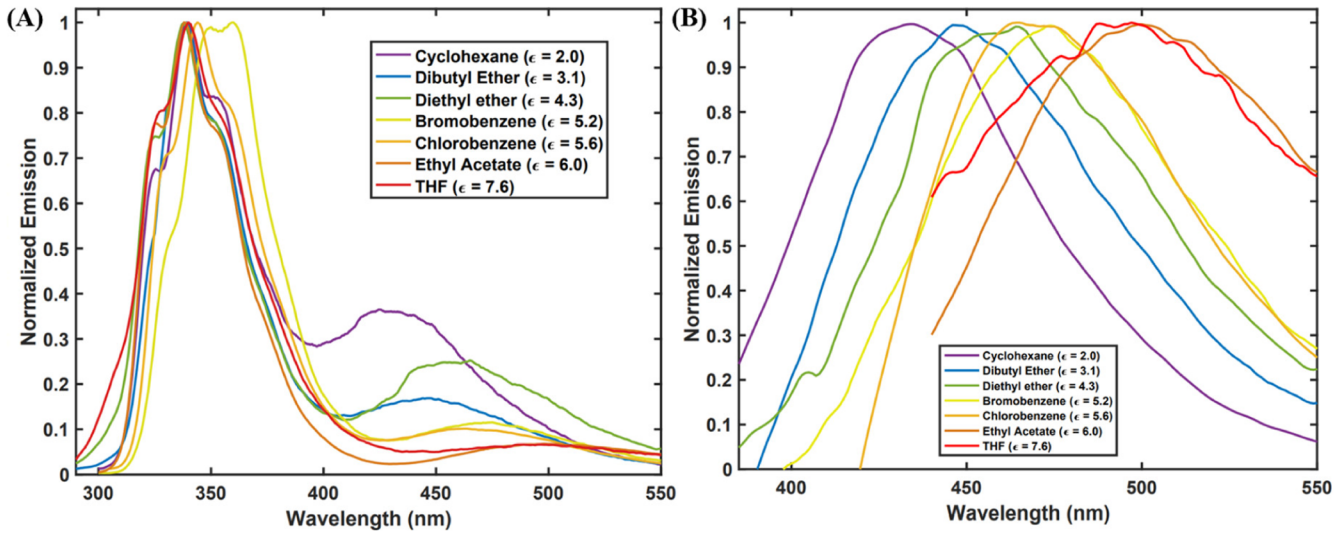

FIG. 1. (a) Fluorescence spectra of OPP-3* in 1.4M TEA with the variation of solvents. (b) Normalized emission of the exciplexes only. Reproduced with permission from Kron *et al.*, J. Phys. Chem. A **126**, 2319–2329 (2022). Copyright 2022 American Chemical Society.

representative geometries are computed by high-throughput geometry optimization starting from over a hundred guess geometries. In this contribution, we report the construction of an automated TDDFT workflow to generate such an ensemble of exciplex structures. The computed geometries are first screened by using known properties of exciplexes and then used to compute emission spectra using Boltzmann weights. We compare the computed emission spectra with prior experiments to determine whether this ensemble-based approach is capable of reproducing the solvatochromic shifts and chain-length dependence ([OPP-3–TEA]* vs [OPP-4–TEA]*) better than a previously employed protocol based on a single structure. We show that this approach indeed leads to a distribution of exciplex geometries with varying CT and emission characteristics and that the fluorescence spectra of exciplex ensembles agree better with experimental observations.

METHODS

Computational methods

The quantum chemistry software package Q-Chem[65] was used for all the linear-response TDDFT[56,66] simulations. We employ the long-range–corrected exchange–correlation energy functional with dispersion correction, ωB97X-D,[67,68] and the 6-311G** basis set. We have chosen cyclohexane (C_6H_{12}) as a representative solvent and described solvation with the implicit conductor-like polarizable continuum model (C-PCM).[69–72]

The most tedious step in the protocol for generating a distribution of geometries to describe the exciplex state is TDDFT optimization of the numerous guess structures (guess generation is described in the following section). Optimization is carried out using a small step size (0.02 a.u.), and tolerance on the maximum gradient component is tightened to 2×10^{-5} a.u. We use full TDDFT in all our calculations, as the Tamm-Dancoff approximation (TDA) was previously shown to be inaccurate.[34] To determine which excited state shows partial CT from TEA → OPP-3*, we compute and analyze the ten lowest singlet excited states. We found that the lowest excited state shows the partial CT character for most guess structures (with some exceptions, described in the Results and Discussion section). In the current protocol, TDDFT optimization follows the first excited state in all cases. The unique optimized structures identified using the screening procedure (described in the next section) are then subjected to vibrational analysis to confirm that they are local minima on the PES.

To analyze inter-fragment interactions in the donor–acceptor complex, [OPP-3–TEA]*, we employ excited-state energy decomposition analysis (exEDA).[50,73] The scheme decomposes excitation energy into frozen (FRZ), polarization (POL), and CT terms using absolutely localized molecular orbitals (ALMOs).[74] Although the current implementation is limited to the isolated species, exEDA serves as a useful tool for verifying the formation of exciplexes.[34,73] Dominant contribution to the excitation energy indicates energy lowering via exciplex formation upon partial electron transfer from TEA to OPP*. Therefore, we have chosen exEDA for distinguishing exciplexes from other excited-state minima by quantifying the CT contribution to excitation (emission) energy.

In addition to exEDA, we carry out excited-state Mulliken population analysis to determine the partial charges on the donor and acceptor fragments in the exciplex.[75] NTO analysis provides another clear indicator of CT and formation of exciplexes.[42,44,76,77] We visualized the hole and electron NTOs, which are extracted from the transition density matrix, using IQmol and Jmol.[78,79] Using NTOs, we also calculate the vectorial electron–hole distance $d_{h\to e}$, an exciton descriptor that represents an average distance between the centroids of electron and hole distributions,[49] as an indicator of exciplex formation. Although visualization of NTOs provides a clear picture of electronic transition, exciton descriptors are particularly useful for automated workflows.

We use the state-specific approach[80] to describe out-of-equilibrium solvent effects on the vertical emission ($S_1 \to S_0$). We quantify the solvatochromism of the exciplex ensemble by calculating vertical emission oscillator strength (f) and emission energies in various solvents. Prior work from our group shows that excimer structures optimized in different solvents described by an implicit solvation model are rather similar.[34] Therefore, the current protocol uses the geometries optimized in cyclohexane (CyHex) and performs single-point calculation of vertical emission energy and oscillator strength with diethyl ether (Et_2O) and dichloromethane (DCM) solvents. The protocol can be easily extended to perform geometry optimization in each solvent, which might become important for other systems and solvents; the effect of solvent-specific optimization will be examined in future work.

All solvents considered in this work and our previous study (Fig. 1) have small dielectric constants because exciplexes are less likely to form in solvents with a higher dielectric constant in which complete electron transfer become more energetically favorable.[34] To generate ensemble spectra in each solvent and compare solvatochromic shifts with experiment, we assume Boltzmann's populations of the exciplex structures by weighting the contribution of each ensemble structure i as follows:

$$p_i = \frac{e^{-(\varepsilon_i - \bar{\varepsilon})/(kT)}}{\sum_j e^{-(\varepsilon_j - \bar{\varepsilon})/(kT)}}, \tag{1}$$

where ε_i is the electronic energy of ith geometry in the first excited state computed in a particular solvent, $\bar{\varepsilon}$ is the mean of energies of 27 geometries, and k is the Boltzmann constant. The temperature is set to 298 K. To plot the spectra, the oscillator strengths of individual transitions are convoluted with Gaussian functions[60] [more information in Sec. S1 in the supplementary material], and the convoluted spectra are then transformed to the wavelength scale (nm).

Implementing workflows for exciplex ensemble generation

Excited-state simulations are more susceptible to errors and require greater computational effort compared with ground-state simulations. In this work, we utilize scientific workflows and error-handling routines to automate these calculations. We use FireWorks[81] to manage all the simulations, and the Custodian[82] error-handling wrapper to perform the Q-Chem calculations. Input/output parsing is performed using the Python Materials Genomics (pymatgen) library.[82] The library contains a Q-Chem

parser for ground-state calculations. We developed a locally modified version of pymatgen to parse excited-state information, construct input files for excited-state property calculations (vibrational analysis, exEDA, NTO, and exciton properties), and perform high-throughput analysis of the output files.

Figure 2 illustrates the sequence of operations carried out to generate the exciplex ensemble for [OPP-3–TEA]*. The procedure is slightly modified for [OPP-4–TEA]* as described below. We construct a set of 130 exciplex guess structures using the structure identified in prior work as the starting point.[34] We generate the guess structures by systematic displacement of the TEA fragment both parallel and perpendicular to the approximate plane of OPP*. Of the 130 guess structures, 8 are constructed by rotation of the three ethyl groups in TEA around the vertical axis defined by the separation between N and the plane of the central ring of OPP. Section S2 in the supplementary material describes the procedure for the construction of guess geometries.

TDDFT optimization is carried out by following the first excited state. Following optimization, duplicate structures are eliminated using pairwise distances and total energies as criteria for comparison. To determine the difference between structures, we use the Eckart distance measure, which is also employed in the double-ended transition state search methods known as the freezing string method.[83,84] By carefully analyzing pairs of computed structures, we find that 1.2 Å is a suitable cutoff value, below which we consider the pair as structurally identical. If this structural criterion is met *and* the energy difference is below 0.05 eV, the higher-energy structure is eliminated as a duplicate. By using these criteria, we identify 41 unique structures.

The next step is to test if the unique complexes are true local minima by checking whether vibrational analysis yields all real frequencies. Of the 41 structures, 7 have one imaginary frequency, ranging between $4i$ and $87i$ cm^{-1}. It is possible to construct a Custodian routine to re-run TDDFT optimization from these geometries,

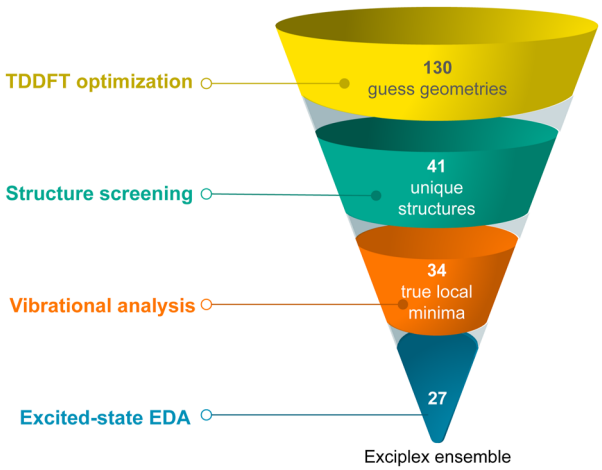

FIG. 2. The screening of unique exciplex structures from 130 initial geometries. The workflow consists of TDDFT optimization, screening out duplicates, excited-state vibrational analysis to verify the minima, and excited-state EDA to verify exciplex character. For [OPP-3-TEA]*, this workflow generated an ensemble of 27 exciplexes.

but in the present study, we simply discard the structures with imaginary frequencies. The final step is to determine whether all 34 local excited-state minima are exciplexes, i.e., that they exhibit significant CT character. Either excited-state Mulliken analysis or exEDA can be used for that purpose. Of the 34 structures, 7 [OPP-3–TEA]* complexes show very low or no CT from TEA to OPP-3. Table S2 of the supplementary material presents the excited-state information for these seven structures, along with the charge on monomers, and the contribution of CT interaction to the excitation energy (from exEDA). We define weak (or negligible) CT by the small ($|q| < 0.1e$) negative (positive) charge on OPP-3* (TEA) and correspondingly small CT contribution to emission energy ($|\Delta E_{CT}| < 0.15$ eV). We find that in these seven complexes, a higher excited state corresponds to TEA → OPP-3* CT; however, these states do not contribute to exciplex emission by virtue of Kasha's rule.

By executing this workflow for 130 structures, we obtain 27 unique excited-state minima exhibiting strong CT character that can, therefore, be classified as exciplexes. The structures of these exciplexes are described in terms of donor–acceptor distance and acceptor dihedral angles in Fig. S2 and Table S1 of the supplementary material.

RESULTS AND DISCUSSION

[OPP-3–TEA]*: Structure and characteristics

Table S3 in the supplementary material reports exciplex characteristics, including electronic energy, fragment charges, exEDA terms, and emission energies. The lowest transition in the optimized exciplex structures has a smaller oscillator strength than the transition in the excited-state optimized isolated OPP-3*. The mean oscillator strength of the exciplex ensemble in cyclohexane is 0.10 (Table S4 in the supplementary material), to be compared with the oscillator strength for OPP-3* emission of 1.32. The exciplex structures with the highest (−986.537 hartree) and lowest (−986.554 hartree) total energies differ by 0.45 eV. Table S3 in the supplementary material reveals that the CT contribution to emission energy (calculated by exEDA) is significantly higher than either frozen or polarization contributions.

Partial CT is also confirmed by excited-state Mulliken population analysis, with the negative charge on the acceptor fragment ranging from −0.79 to −0.93e. The mean electron–hole distance ($d_{h\to e}$) for the exciplex ensemble of [OPP-3–TEA]* is 2.61 Å, which is significantly larger than $d_{h\to e}$ in the isolated OPP-3* ($d_{h\to e} < 0.5$ Å) characterizing intramolecular CT.

Figure 3 shows the NTOs of the exciplexes with the highest (3.15 eV) and lowest (2.72 eV) emission energies. The hole NTO is centered around the TEA nitrogen, and the particle NTO spans two consecutive phenyl rings of the OPP-3 fragment.

[OPP-3–TEA]*: Fluorescence and solvatochromism

Table S3 in the supplementary material shows that the ensemble of exciplexes generated in this work exhibits a range of emission energies from 2.72 to 3.15 eV. Since red-shifted emission energy relative to isolated OPP-3* is a direct consequence of CT-driven stabilization of the complex, it is not surprising that the emission energy exhibits a linear correlation with the ΔE_{CT} term from exEDA, which is shown in Fig. S3 in the supplementary material.

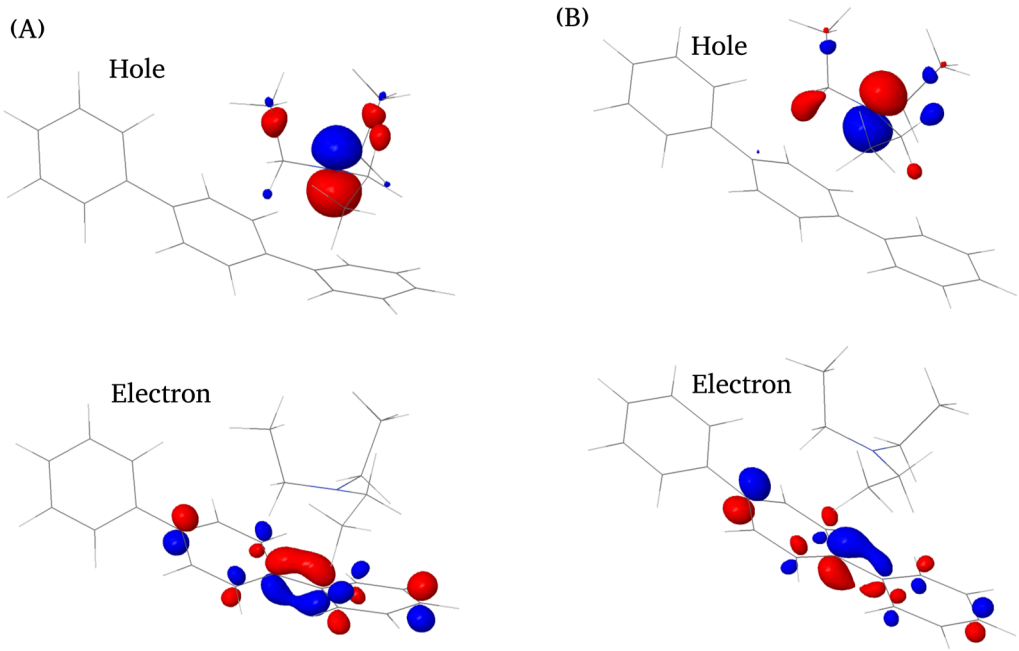

FIG. 3. NTOs for two representative [OPP-3–TEA]* exciplex structures. (a) Exciplex with the lowest (393 nm) emission wavelength. (b) Exciplex with the highest (457 nm) wavelength. The electron–hole distances, $d_{h\to e}$, are 2.69 and 2.38 Å for (a) and (b), respectively.

In other words, redder emission results from a greater CT-driven stabilization of the exciplex.

To compute emission spectra, we use TDDFT vertical transition energies and the respective oscillator strengths.[39,85–87] Figure 4 shows the fluorescence stick spectra of the individual structures (plotted against the emission wavelength, λ, nm) for solvents with dielectric constants increasing from the left to the right. Table S4 in the supplementary material reports the emission wavelengths and corresponding oscillator strengths. As observed experimentally (Fig. 1), the exciplex signature or the range of emission wavelengths red-shifts with the increasing solvent dielectric constant. This can be explained by the reduced energy gap in a higher dielectric solvent due to favorable solvation of the excited state because of its partial CT character.[88,89]

Figure 5 shows Boltzmann-weighted exciplex fluorescence spectra for CyHex, Et_2O, and DCM solvents assuming small broadening (σ = 0.05 eV). Compared with the unweighted stick spectra shown in Fig. 4, the peak shifts to a longer wavelength for every solvent. When compared with the experimental spectra in Fig. 1, it is evident that reproducing the broad exciplex feature requires a larger value of σ. Nevertheless, Fig. 5 is instructive and indicates that experimentally observed solvatochromism is also qualitatively reproduced by the exciplex ensemble.

Table I compares experimental peak positions and shifts with the calculated shift for a single exciplex structure reported in our prior work and the current study using the ensemble-based protocol. The mean absolute deviation from experimental emission peaks is lower for the ensemble treatment with broadening (12 nm,

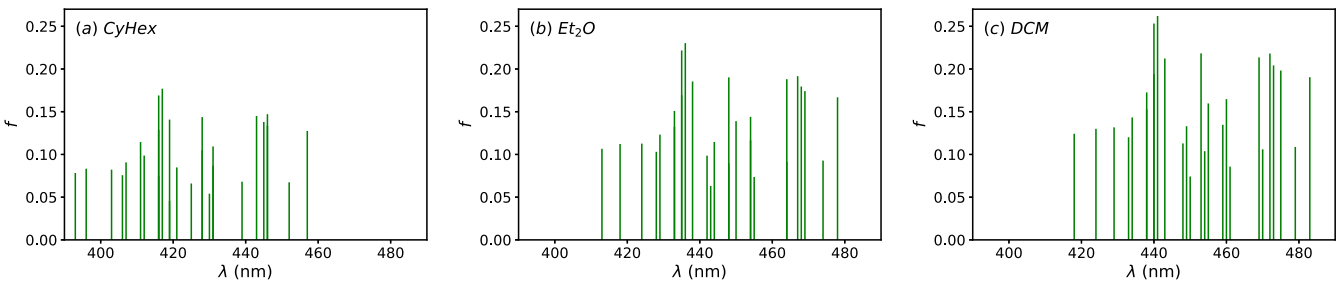

FIG. 4. Stick spectra of 27 unique exciplex structures for solvents of varying dielectric: (a) Cyclohexane (ε = 2.02), (b) diethyl ether (ε = 4.34), and (c) dichloromethane (ε = 8.93).

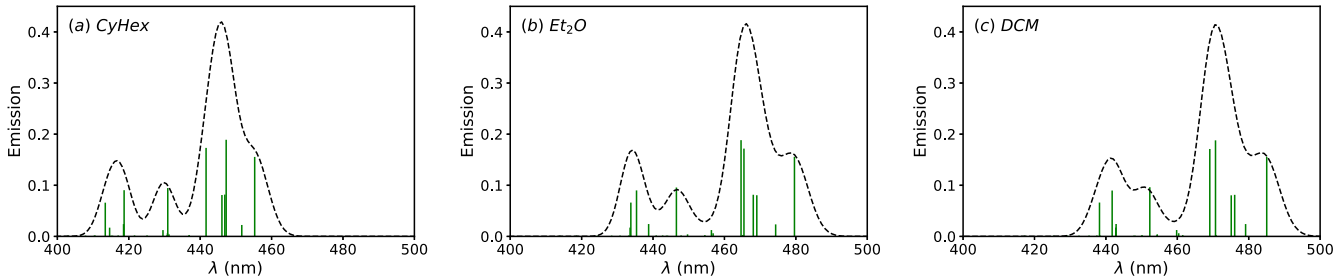

FIG. 5. Energy-weighted stick spectra of 27 unique exciplex structures plotted against the emission wavelength (in nm) for (a) cyclohexane ($\varepsilon = 2.02$), (b) diethyl ether ($\varepsilon = 4.34$), and (c) dichloromethane ($\varepsilon = 8.93$). Width $\sigma = 0.05$ eV is used to broaden the spectra (black dashed). The spectra are re-scaled for ease of visualization.

TABLE I. Comparison of experimental emission peaks (nm) with our prior study employing a single structure protocol ("Calculated, single"), and the current work using an ensemble of exciplex structures ("Calculated, ensemble"). The columns labeled "shift" refer to the solvatochromic shift between CyHex → Et_2O and Et_2O → DCM. The band maxima and shifts in eV are reported in parentheses.

	Experiment[34]		Calculated, single[34]		Calculated, ensemble[a]		Calculated, ensemble ($\sigma = 0.4$ eV)[b]	
Solvent	λ	Shift	λ	Shift	λ	Shift	λ	Shift
CyHex	428 (2.89)		421 (2.94)		446 (2.78)		441 (2.81)	
Et_2O	460 (2.69)	32 (0.20)	442 (2.80)	21 (0.14)	467 (2.65)	21 (0.13)	461 (2.69)	20 (0.12)
DCM	489 (2.53)	29 (0.16)	448 (2.76)	6 (0.04)	472 (2.62)	5 (0.03)	466 (2.66)	5 (0.03)

[a]The maximum oscillator strength in the Boltzmann-weighted distribution with no broadening ($\sigma = 0$ eV).
[b]Peak position and shifts from the ensemble of exciplex structures with the broadening of $\sigma = 0.4$ eV.

0.07 eV) compared with a single structure (22 nm and 0.13 eV). An ensemble-based protocol, however, does not improve the accuracy of computed solvatochromic shifts.

We examine the possible role of the choice of implicit solvation model on solvatochromic shifts. A prior study has shown that the SMD model (solvation model based on charge density) for implicit solvation[90] yields better agreement with experimental solvatochromic shifts than C-PCM in the absorption spectrum of a solvatochromic probe molecule, N,N-diethyl-4-nitroaniline.[91] These differences in model performance likely originate in their respective choices of atomic radii and cavity construction method.[90,91] When employed to construct Boltzmann-weighted and broadened (σ = 0.4 eV) fluorescence spectra for the exciplex ensemble, SMD yields emission peaks at 447, 465, and 476 nm (2.77, 2.66, and 2.60 eV) for CyHex, Et_2O, and DCM, respectively, with DCM showing the highest difference between SMD and PCM peaks. The resulting solvatochromic shifts are 18 nm (0.11 eV) and 11 nm (0.06 eV). Thus, the SMD model yields emission wavelengths that are red-shifted relative to the PCM values and performs marginally better than the latter in predicting the solvatochromic shift between Et_2O and DCM. The trends in solvatochromic shifts and deviations of PCM and SMD from the experiment agree with the study of vertical excitation energies of N,N-diethyl-4-nitroaniline using state-specific solvation models.[91]

The preceding analysis shows that our ensemble approach to modeling exciplexes is not sufficient to completely capture the solvent effects and that a refinement of the protocol for exciplex calculations and solvent models is necessary. In the present workflow, we use a single ensemble calculated in CyHex and only include solvent effects through single-point excitation energy calculations, based on our prior work,[34] where we observed that the solvent does not affect the resulting excimer structures. Thus, our protocol does not account for possible new structures that may arise in other solvents. In addition to the solvents examined with the ensemble approach, we noted in our previous work (using a single representative exciplex structure) that modeling solvent as a dielectric continuum fails to capture anomalous red shift observed in the exciplex emission from the aromatic solvent chlorobenzene (ϵ = 5.6) to bromobenzene (ϵ = 5.2).[34] We tentatively attributed this discrepancy to the effect of π-stacking interactions between the solvents and OPP*.

It is very likely that a complete description of solvatochromism in exciplexes requires an ensemble representation of the entire system, including both the solvent and the solute. A prior study qualitatively reproduced trends in solvatochromism in vertical absorption by explicitly modeling the solvation shell using hundreds of solvent molecules and constructing the ensemble using snapshots from molecular dynamics trajectories.[91] However, quantitative agreement was not achieved as smaller basis sets were employed to keep the cost of simulation of these large models reasonable. A spectra study of 5-methylcytidine, which is capable of hydrogen bonding with solvent, shows that pure quantum mechanics (QM), hybrid quantum mechanics/molecular mechanics (QM/MM), and QM/MM models with molecular dynamics all yield absorption spectra and solvatochromism with reasonable accuracy, although the latter also captures spectral shapes better.[92] QM/MM models with polarizable embedding employed in conjunction with molecular dynamics also have been shown to reliably predict solvatochromic

shifts in the absorption wavelength of small molecules.[93] Although vertical absorption simulations are based molecular dynamics sampling of the ground-state configurations, extending this approach to ensemble simulations of exciplex emission would involve QM/MM *ab initio* molecular dynamics simulations, which is more computationally demanding. In addition to higher computational costs relative to absorption simulation, this requires careful screening of excited-state dynamics snapshots to identify only those that possess partial CT character.

Figure 6 shows the ensemble-averaged spectra superimposed with the normalized experimental emission for CyHex and Et_2O, with the latter chosen owing to a sharper experimental peak position compared with solvents of a higher dielectric. The emission wavelengths corresponding to the highest oscillator strength in the Boltzmann-weighted spectra are shown using blue-dashed lines. A Gaussian broadening width of $\sigma = 0.4$ eV is used for the comparison. The impact of increasing σ on the calculated spectrum is compared against the exciplex part of the full fluorescence spectra in Fig. S5 in the supplementary material. Considering the broad characteristics of the experimental emission spectra, it is more appropriate to utilize calculated spectra with a broadening of $\sigma = 0.4$ eV, rather than a distribution without any broadening. Table I shows the associated peaks for different solvents and solvatochromic shifts.

The peak positions of broadened spectra ($\sigma = 0.4$) are at 441 and 461 nm (2.81 and 2.68 eV) for CyHex and Et_2O solvents, respectively, which are red-shifted relative to the experimental emission peaks by about 13 and 1 nm (0.08 and 0.01 eV) and agree better than the peak positions in the unbroadened spectra (Table I).

One possible limitation of our approach is that the configurational space of exciplexes spanned is not complete, something that can be partially remedied going forward by re-optimization of the structures that were screened out owing to imaginary frequencies. In addition, we note that our approach assumes complete thermalization of the excited states. To explore these issues, we are carrying out *ab initio* molecular dynamics simulations on the excited state PES; the results of this study will be reported elsewhere. Nevertheless, the ensemble generated in this study encompasses exciplex geometries that may be structurally difficult to distinguish but possess a wide range of emission energies. This range may be sufficient to reproduce experimentally observed spectra, although capturing solvent dependence will require the exploration of alternative implicit or explicit solvation models.

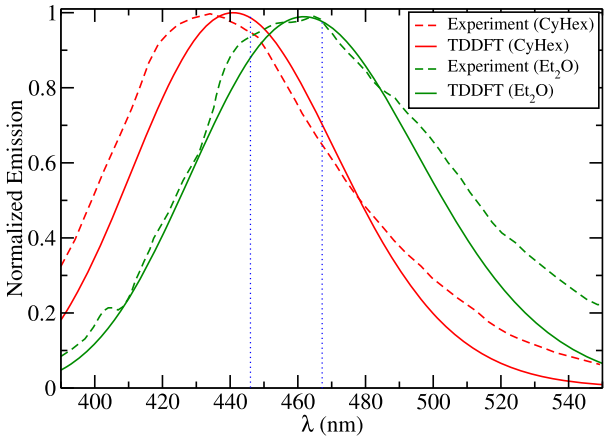

FIG. 6. A comparison of ensemble-averaged spectra obtained from TDDFT calculation and normalized experimental emission spectra in CyHex and Et_2O solvents. We use $\sigma = 0.4$ eV for broadening. The heights of the peaks are adjusted to appear comparable with the experiment. The emission wavelengths corresponding to the highest oscillator strength in the energy-weighted but not broadened spectra ($\sigma = 0$ eV) are marked with blue-dotted lines.

[OPP-4–TEA]*: Modified workflows and fluorescence

We extended the exciplex generation workflow to [OPP-4–TEA]*, motivated by unsatisfactory results of our prior work—that a single structure-based analysis yields very similar emission energies for [OPP-4–TEA]* and [OPP-3–TEA]*, in disagreement with experimental observation of longer experimental fluorescence wavelengths for the former across various solvents.[34] Here, we employ a slightly modified procedure derived from the procedure used to construct the [OPP-3–TEA]* ensemble. Specifically, we used 27 distinct exciplex geometries of [OPP-3–TEA]* to generate guess structures for [OPP-4–TEA]* by adding a fourth phenyl group. For each of these structures, a phenyl group was appended to terminal phenyl groups of OPP-3 in the +ve x-direction (Fig. S1). To account for the additional degrees of freedom due to the fourth phenyl group, 24 more geometries were constructed by placing the TEA with its N atom positioned atop specific carbon atoms separated by ≈3 Å. Of these 24 structures, six consist of TEA ethyl groups rotated symmetrically by ≈60° about the vertical axis passing through the N atom. Further details of [OPP-4–TEA]* guess structure generation are provided in Sec. S6 in the supplementary material.

Figure 2 illustrates the remaining workflow steps of the calculation—TDDFT following the first excited state and the verification of the exciplex character. Of the 40 unique geometries obtained after eliminating duplicates, 34 local minima were identified using vibrational analysis, of which 25 exhibit significant CT. We note that of the 51 guesses, the first excited state (although followed in TDDFT optimization) does not correspond to the exciplex or CT state in 9 geometries.

Table S5 in the supplementary material describes the characteristics of the [OPP-4–TEA]* exciplexes. Similar to [OPP-3–TEA]*, the first excited state of [OPP-4–TEA]* is the exciplex state. The orbital picture in Fig. S7 in the supplementary material confirms that partial CT occurs from TEA to OPP-4, and the particle NTOs are localized to two consecutive phenyl rings, similar to [OPP-3–TEA]* (Fig. 3). Table S6 in the supplementary material reports emission wavelength and oscillator strengths of [OPP-4–TEA]* exciplexes in three solvents. In addition to comparing the [OPP-4–TEA]* TDDFT spectra (Fig. S8 in the supplementary material and Fig. 7) with experiment, we assess whether the ensemble-averaged spectra can explain the experimentally observed red-shift relative to [OPP-3–TEA]*.

Although it is difficult to compare structures on a one-to-one basis, the emission wavelengths of [OPP-4–TEA]* (Table S5 in the supplementary material) differ by −8 to 53 nm from the [OPP-3–TEA]* (Table S3 in the supplementary material)

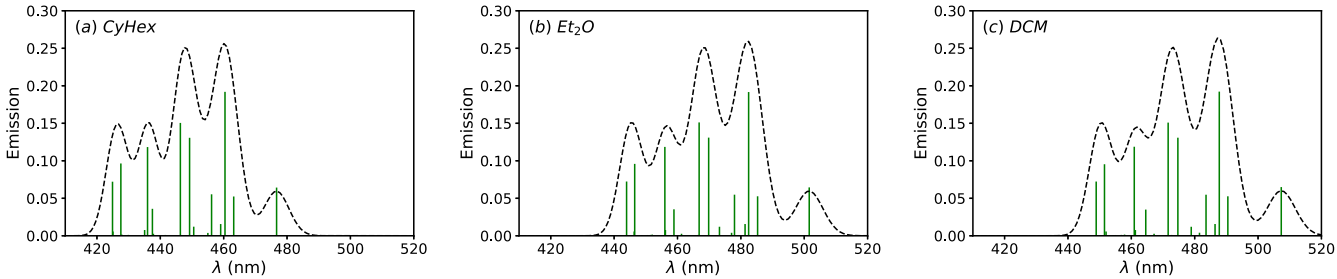

FIG. 7. Energy-weighted stick spectra (green sticks) of 25 unique [OPP-4–TEA]* exciplex structures vs emission wavelengths (in nm) (a) Cyclohexane ($\varepsilon = 2.02$), (b) diethyl ether ($\varepsilon = 4.34$), and (c) dichloromethane ($\varepsilon = 8.93$). The broadening width $\sigma = 0.05$ eV is used to plot the spectra (black dashed). Peak heights are scaled for better visualization against the stick spectra.

ensemble. This is a clear indication that a single geometry is insufficient to describe the experimentally observed impact of acceptor chain length on exciplex emission wavelength and that an ensemble of geometries is required. Table II describes the differences in emission characteristics observed with increasing chain length of the acceptor. The experimental peaks for [OPP-4–TEA]* are at 444, 470, and 503 nm (2.79, 2.64, and 2.46 eV) in CyHex, Et_2O, and DCM, respectively, red-shifted relative to [OPP-3–TEA]* by 16, 10, and 14 nm (0.10, 0.05, and 0.07 eV). The positions of the largest energy-weighted transition (which represents the emission band maxima) obtained with the exciplex ensemble are 460, 483, and 488 nm (2.69, 2.56, and 2.54 eV), respectively. With the exception of DCM, calculated emission peaks are at longer wavelengths compared with experiment. The differences between the computed band maxima of [OPP-4–TEA]* and [OPP-3–TEA]*—14, 16, and 16 nm (0.10, 0.07, and 0.07 eV), respectively—are in excellent agreement with experiment.

As the change in broadening going from the [OPP-3–TEA]* to [OPP-4–TEA]* exciplex is not known, we assume the same broadening ($\sigma = 0.4$ eV) to calculate convoluted spectra for the latter. Figure S9 in the supplementary material compares the two exciplex ensembles. The peaks of the resulting spectra are at 448, 469, and 474 nm (2.76, 2.64, and 2.61 eV), with smaller differences between them compared with the differences in unbroadened peak maxima (Table II).

Therefore, although the ensemble model of an exciplex brings us closer to experimentally observed fluorescence characteristics compared with the single-structure representation used in prior work by our group,[34] discrepancies persist. They could be due to the choice of solvation model, as we discussed above, or due to an incomplete search space, particularly toward the longer wavelength limit of the fluorescence spectrum. Going forward, the latter hypothesis will be examined by comparing our results with those obtained from the *ab initio* molecular dynamics simulations. Finally, the limitations of the employed quantum-chemistry method (TDDFT) can be partially responsible for the remaining discrepancies—although we used one of the best long-range functionals (ωB97X-D) in which self-interaction error (SIE) is much smaller than in, for example, B3LYP, where it is not completely eliminated. In a future study, we will explore the effect of the residual SIE on exciplex properties.

Efficient workflows: Future work

We demonstrated that workflows can be employed to streamline otherwise tedious TDDFT calculations and verification of excited-state CT complexes. Our work also clearly illustrated that an exciplex state cannot be completely represented by a single geometry. A distribution of structures brings computational predictions of spectral features and chain-length dependence closer to experiment than the use of a single representative geometry. One limitation of our approach lies in the first step of the workflow. We assumed that the first excited state corresponds to the exciplex state in the guess structure, which is the mode that is followed in the course of TDDFT optimization. However, this is not always true, as we found even in this study for both exciplex ensembles, and cannot be generalized across different levels of theory. Therefore, our main goal going forward is to improve the workflow implementation. An excited-state Mulliken charge analysis on the guess structure will determine

TABLE II. Difference between emission wavelengths (nm) of [OPP-4–TEA]* and [OPP-3–TEA]* exciplexes obtained from (a) Experiment,[34] (b) single structure,[34] (c) ensemble peak (without broadening, $\sigma = 0$ eV), and (d) ensemble fluorescence peak ($\sigma = 0.4$ eV). The differences in eV are reported in parentheses.

Solvent	Experiment	Single structure	Ensemble peak ($\sigma = 0$ eV)	Ensemble peak ($\sigma = 0.4$ eV)
CyHex	16 (0.10)	1 (0.01)	14 (0.10)	7 (0.043)
Et_2O	10 (0.05)	−1 (−0.01)	16 (0.07)	8 (0.045)
DCM	14 (0.07)	−2 (−0.01)	16 (0.07)	8 (0.045)

whether the first excited state corresponds to a partial CT state, and we will apply the subsequent TDDFT optimization and characterization steps of the workflow only to those structures that satisfy this criterion. Such workflows will eliminate the optimization of states that have no CT character. Furthermore, following existing routines for ground-state optimizations, we will implement Custodian routines to restart TDDFT optimization jobs for those that yield one or more imaginary vibrational modes.

CONCLUSIONS

In this work, we tested our hypothesis that the red-shifted broad fluorescence band characteristic of exciplexes in general, and the [OPP–TEA]* partial CT complex, in particular, is the result of the emission of a distribution or ensemble of geometries. We developed an ensemble-based protocol in which exciplexes are screened using high-throughput Q-Chem calculations. This is accomplished by means of modifications to a local version of the pymatgen software for parsing excited-state input/output and the use of FireWorks to construct workflows for excited-state optimization and exciplex verification and Custodian for error handling. Of the 130 initial geometries, we successfully identified 27 unique [OPP-3–TEA]* exciplex structures by systematically screening out duplicates, verifying minima, and identifying those with strong CT character using tools including exEDA, NTO, and excited-state Mulliken analysis. We constructed the fluorescence spectra by Boltzmann-weighting individual structures. These spectra agree better with experiment than the spectra computed for a single exciplex geometry identified in prior work in our group. However, we believe that in order to accurately describe solvatochromism, alternative solvation models beyond C-PCM are necessary. We extended this workflow to calculate the [OPP-4–TEA]* exciplex ensemble, which resulted in 25 unique geometries. Once again, a distribution of structures provides a significantly improved description of the exciplex state than a single structure. This is illustrated by the computed red shifts of [OPP-4–TEA]* relative to [OPP-3–TEA]* in various solvents for which the ensemble approach agrees better with experiments.

SUPPLEMENTARY MATERIAL

The supplementary material contains excited-state properties of [OPP-3–TEA]* and [OPP-4–TEA]* exciplexes. The structural information of exciplexes, NTOs showing the hole and electron orbitals, and emission spectra for [OPP-4–TEA]* are also available.

ACKNOWLEDGMENTS

This work was supported by the U.S. Department of Energy, Office of Science, Office of Basic Energy Sciences under Award No. DE-SC0022326. The authors also acknowledge computational resources and support from USC's Center for Advanced Research Computing (CARC) and the National Energy Research Scientific Computing Center (NERSC). The authors are grateful to Professor Jahan Dawlaty (USC), George Baffour Pipim (USC), and Goran Giudetti (USC) for helpful discussions.

AUTHOR DECLARATIONS

Conflict of Interest

The authors have no conflicts to disclose.

Author Contributions

Abhilash Patra: Data curation (lead); Formal analysis (lead); Investigation (lead); Methodology (lead); Resources (equal); Software (equal); Visualization (equal); Writing – original draft (equal); Writing – review & editing (equal). **Anna I. Krylov**: Conceptualization (equal); Funding acquisition (lead); Methodology (equal); Project administration (equal); Supervision (equal); Writing – review & editing (supporting). **Shaama Mallikarjun Sharada**: Conceptualization (equal); Funding acquisition (supporting); Investigation (equal); Methodology (equal); Project administration (equal); Supervision (equal); Writing – original draft (equal); Writing – review & editing (equal).

DATA AVAILABILITY

The data that support the findings of this study are available within the article and its supplementary material. The exciplex geometries are available in the manuscript. The authors' modified pymatgen code for excited states is available on request.

REFERENCES

[1] N. J. Turro, V. Ramamurthy, and J. Scaiano, *Modern Molecular Photochemistry of Organic Molecules* (University Science Books, Mill Valley, 1991).
[2] T. Förster, "Excimers," Angew. Chem., Int. Ed. **8**, 333–343 (1969).
[3] S. L. Mattes and S. Farid, "Exciplexes and electron transfer reactions," Science **226**, 917–921 (1984).
[4] J. B. Birks, "Excimers," Rep. Prog. Phys. **38**, 903 (1975).
[5] K. Diri and A. I. Krylov, "Electronic states of the benzene dimer: A simple case of complexity," J. Phys. Chem. A **116**, 653–662 (2011).
[6] X. Feng, A. V. Luzanov, and A. I. Krylov, "Fission of entangled spins: An electronic structure perspective," J. Phys. Chem. Lett. **4**, 3845–3852 (2013).
[7] *Principles of Fluorescence Spectroscopy*, edited by J. R. Lakowicz (Springer, Boston, MA, 2006), pp. 277–330.
[8] D. Setiawan, D. Sethio, M. A. Martoprawiro, and M. Filatov, "Formation of bonded exciplex in the excited states of dicyanoanthracene-pyridine system: Time dependent density functional theory study," in *Proceedings of the 2011 2nd International Congress on Computer Applications and Computational Science* (Springer, Berlin, Heidelberg, 2012), pp. 403–409.
[9] Y. Wang, O. Haze, J. P. Dinnocenzo, S. Farid, R. S. Farid, and I. R. Gould, "Bonded exciplexes. A new concept in photochemical reactions," J. Org. Chem. **72**, 6970–6981 (2007).
[10] D. Casanova, "Theoretical investigations of the perylene electronic structure: Monomer, dimers, and excimers," Int. J. Quantum Chem. **115**, 442–452 (2015).
[11] N. O. Dubinets, A. A. Safonov, and A. A. Bagaturyants, "Structures and binding energies of the naphthalene dimer in its ground and excited states," J. Phys. Chem. A **120**, 2779–2782 (2016).
[12] E. S. S. Iyer, A. Sadybekov, O. Lioubashevski, A. I. Krylov, and S. Ruhman, "Rewriting the story of excimer formation in liquid benzene," J. Phys. Chem. A **121**, 1962–1975 (2017).
[13] Y. Gao, H. Liu, S. Zhang, Q. Gu, Y. Shen, Y. Ge, and B. Yang, "Excimer formation and evolution of excited state properties in discrete dimeric stacking of an anthracene derivative: A computational investigation," Phys. Chem. Chem. Phys. **20**, 12129–12137 (2018).
[14] S. Reiter, M. K. Roos, and R. de Vivie-Riedle, "Excited state conformations of bridged and unbridged pyrene excimers," ChemPhotoChem **3**, 881–888 (2019).

[15]R. A. Krueger and G. Blanquart, "Exciplex stabilization in asymmetric acene dimers," J. Phys. Chem. A **123**, 1796–1806 (2019).
[16]A. C. Hancock and L. Goerigk, "Noncovalently bound excited-state dimers: A perspective on current time-dependent density functional theory approaches applied to aromatic excimer models," RSC Adv. **12**, 13014–13034 (2022).
[17]J. Lee, B. Kim, J. E. Kwon, J. Kim, D. Yokoyama, K. Suzuki, H. Nishimura, A. Wakamiya, S. Y. Park, and J. Park, "Excimer formation in organic emitter films associated with a molecular orientation promoted by steric hindrance," Chem. Commun. **50**, 14145–14148 (2014).
[18]J. Lee, H. Jung, H. Shin, J. Kim, D. Yokoyama, H. Nishimura, A. Wakamiya, and J. Park, "Excimer emission based on the control of molecular structure and intermolecular interactions," J. Mater. Chem. C **4**, 2784–2792 (2016).
[19]Y.-H. Chen, K.-C. Tang, Y.-T. Chen, J.-Y. Shen, Y.-S. Wu, S.-H. Liu, C.-S. Lee, C.-H. Chen, T.-Y. Lai, S.-H. Tung, R.-J. Jeng, W.-Y. Hung, M. Jiao, C.-C. Wu, and P.-T. Chou, "Insight into the mechanism and outcoupling enhancement of excimer-associated white light generation," Chem. Sci. **7**, 3556–3563 (2016).
[20]Q. Wang, Q.-S. Tian, Y.-L. Zhang, X. Tang, and L.-S. Liao, "High-efficiency organic light-emitting diodes with exciplex hosts," J. Mater. Chem. C **7**, 11329–11360 (2019).
[21]J. Li, Z. Li, H. Liu, H. Gong, J. Zhang, and Q. Guo, "Advances in blue exciplex–based organic light-emitting materials and devices," Front. Chem. **10**, 952116 (2022).
[22]N. V. Korovina, S. Das, Z. Nett, X. Feng, J. Joy, R. Haiges, A. I. Krylov, S. E. Bradforth, and M. E. Thompson, "Singlet Fission in a covalently linked cofacial alkynyltetracene dimer," J. Am. Chem. Soc. **138**, 617–627 (2016).
[23]X. Feng and A. I. Krylov, "On couplings and excimers: Lessons from studies of singlet fission in covalently linked tetracene dimers," Phys. Chem. Chem. Phys. **18**, 7751–7761 (2016).
[24]N. V. Korovina, J. Joy, X. Feng, C. Feltenberger, A. I. Krylov, S. E. Bradforth, and M. E. Thompson, "Linker-dependent singlet fission in tetracene dimers," J. Am. Chem. Soc. **140**, 10179–10190 (2018).
[25]R. Martínez-Máñez and F. Sancenón, "Fluorogenic and chromogenic chemosensors and reagents for anions," Chem. Rev. **103**, 4419–4476 (2003).
[26]J.-S. Wu, J.-H. Zhou, P.-F. Wang, X.-H. Zhang, and S.-K. Wu, "New fluorescent chemosensor based on exciplex signaling mechanism," Org. Lett. **7**, 2133–2136 (2005).
[27]G. Zhang, G. Yang, S. Wang, Q. Chen, and J. Ma, "A highly fluorescent anthracene-containing hybrid material exhibiting tunable blue–green emission based on the formation of an unusual 'T-shaped' excimer," Chem. Eur. J. **13**, 3630–3635 (2007).
[28]B. Valeur and I. Leray, "Design principles of fluorescent molecular sensors for cation recognition," Coord. Chem. Rev. **205**, 3–40 (2000).
[29]J. S. Kim and D. T. Quang, "Calixarene-derived fluorescent probes," Chem. Rev. **107**, 3780–3799 (2007).
[30]Y. Wang, J. Chen, Y. Chen, W. Li, and C. Yu, "Polymer-induced perylene probe excimer formation and selective sensing of DNA methyltransferase activity through the monomer–excimer transition," Anal. Chem. **86**, 4371–4378 (2014).
[31]G. Han, D. Kim, Y. Park, J. Bouffard, and Y. Kim, "Excimers beyond pyrene: A far-red optical proximity reporter and its application to the label-free detection of DNA," Angew. Chem., Int. Ed. **54**, 3912–3916 (2015).
[32]K. J. Kron, A. Rodriguez-Katakura, R. Elhessen, and S. Mallikarjun Sharada, "Photoredox chemistry with organic catalysts: Role of computational methods," ACS Omega **6**, 33253–33264 (2021).
[33]M. Yamawaki, A. Asano, T. Furutani, Y. Izumi, Y. Tanaka, K. Osaka, T. Morita, and Y. Yoshimi, "Photoinduced electron transfer-promoted reactions using exciplex-type organic photoredox catalyst directly linking donor and acceptor arenes," Molecules **24**, 4453 (2019).
[34]K. J. Kron, J. R. Hunt, J. M. Dawlaty, and S. Mallikarjun Sharada, "Modeling and characterization of exciplexes in photoredox CO_2 reduction: Insights from quantum chemistry and fluorescence spectroscopy," J. Phys. Chem. A **126**, 2319–2329 (2022).
[35]A. A. Safonov, A. A. Bagaturyants, and V. A. Sazhnikov, "Fluorescence spectra of (dibenzoylmethanato)boron difluoride exciplexes with aromatic hydrocarbons: A theoretical study," J. Phys. Chem. A **119**, 8182–8187 (2015).
[36]R. Huenerbein and S. Grimme, "Time-dependent density functional study of excimers and exciplexes of organic molecules," Chem. Phys. **343**, 362–371 (2008).
[37]D. Kim, "A density functional theory study of an exciplex: Pyridine and benzene," Bull. Korean Chem. Soc. **39**, 882–886 (2018).
[38]J. Hoche, H.-C. Schmitt, A. Humeniuk, I. Fischer, R. Mitrić, and M. I. S. Röhr, "The mechanism of excimer formation: An experimental and theoretical study on the pyrene dimer," Phys. Chem. Chem. Phys. **19**, 25002–25015 (2017).
[39]L. T. Bergendahl and M. J. Paterson, "Excited states of porphyrin and porphycene aggregates: Computational insights," Comput. Theor. Chem. **1040–1041**, 274–286 (2014).
[40]M. T. do Casal and T. M. Cardozo, "Impact of low-cost methods in the description of excimer and exciplex formation: Pyrene–pyrene and pyrene–naphthalene case studies," Theor. Chem. Acc. **139**, 144 (2020).
[41]N. De Mitri, S. Monti, G. Prampolini, and V. Barone, "Absorption and emission spectra of a flexible dye in solution: A computational time-dependent approach," J. Chem. Theory Comput. **9**, 4507–4516 (2013).
[42]A. V. Luzanov, A. A. Sukhorukov, and V. É. Umanskii, "Application of transition density matrix for analysis of excited states," Theor. Exp. Chem. **10**, 354–361 (1976) [Teor. Eksp. Khim. 10, 456 (1974) (in Russian)].
[43]M. Head-Gordon, A. M. Grana, D. Maurice, and C. A. White, "Analysis of electronic transitions as the difference of electron attachment and detachment densities," J. Phys. Chem. **99**, 14261–14270 (1995).
[44]R. L. Martin, "Natural transition orbitals," J. Chem. Phys. **118**, 4775–4777 (2003).
[45]F. Plasser, M. Wormit, and A. Dreuw, "New tools for the systematic analysis and visualization of electronic excitations. I. Formalism," J. Chem. Phys. **141**, 024106–024113 (2014).
[46]F. Plasser, A. I. Krylov, and A. Dreuw, "libwfa: Wavefunction analysis tools for excited and open-shell electronic states," Wiley Interdiscip. Rev.: Comput. Mol. Sci. **12**, e1595 (2022).
[47]A. I. Krylov, "From orbitals to observables and back," J. Chem. Phys. **153**, 080901 (2020).
[48]S. A. Bäppler, F. Plasser, M. Wormit, and A. Dreuw, "Exciton analysis of many-body wave functions: Bridging the gap between the quasiparticle and molecular orbital pictures," Phys. Rev. A **90**, 052521 (2014).
[49]S. A. Mewes, F. Plasser, A. Krylov, and A. Dreuw, "Benchmarking excited-state calculations using exciton properties," J. Chem. Theory Comput. **14**, 710–725 (2018).
[50]Q. Ge, Y. Mao, and M. Head-Gordon, "Energy decomposition analysis for exciplexes using absolutely localized molecular orbitals," J. Chem. Phys. **148**, 064105 (2018).
[51]R. Cammi and J. Tomasi, "Nonequilibrium solvation theory for the polarizable continuum model: A new formulation at the SCF level with application to the case of the frequency-dependent linear electric response function," Int. J. Quantum Chem. **56**, 465–474 (1995).
[52]M. Cossi and V. Barone, "Separation between fast and slow polarizations in continuum solvation models," J. Phys. Chem. A **104**, 10614–10622 (2000).
[53]Z.-Q. You, J.-M. Mewes, A. Dreuw, and J. M. Herbert, "Comparison of the Marcus and Pekar partitions in the context of non-equilibrium, polarizable-continuum solvation models," J. Chem. Phys. **143**, 204104 (2015).
[54]J.-M. Mewes, Z.-Q. You, M. Wormit, T. Kriesche, J. M. Herbert, and A. Dreuw, "Experimental benchmark data and systematic evaluation of two *a posteriori*, polarizable-continuum corrections for vertical excitation energies in solution," J. Phys. Chem. A **119**, 5446–5464 (2015).
[55]E. Stendardo, F. Avila Ferrer, F. Santoro, and R. Improta, "Vibrationally resolved absorption and emission spectra of dithiophene in the gas phase and in solution by first-principle quantum mechanical calculations," J. Chem. Theory Comput. **8**, 4483–4493 (2012).
[56]C. Adamo and D. Jacquemin, "The calculations of excited-state properties with time-dependent density functional theory," Chem. Soc. Rev. **42**, 845–856 (2013).
[57]F. Santoro and D. Jacquemin, "Going beyond the vertical approximation with time-dependent density functional theory," Wiley Interdiscip. Rev.: Comput. Mol. Sci. **6**, 460–486 (2016).
[58]J. Greiner and D. Sundholm, "Calculation of vibrationally resolved absorption and fluorescence spectra of the rylenes," Phys. Chem. Chem. Phys. **22**, 2379–2385 (2020).

[59]S. Hammer, T. Linderl, K. Tvingstedt, W. Brütting, and J. Pflaum, "Spectroscopic analysis of vibrational coupling in multi-molecular excited states," Mater. Horiz. **10**, 221–234 (2023).
[60]S. Gozem and A. I. Krylov, "The ezSpectra suite: An easy-to-use toolkit for spectroscopy modeling," Wiley Interdiscip. Rev.: Comput. Mol. Sci. **12**, e1546 (2022).
[61]S. Di Grande, I. Ciofini, C. Adamo, M. Pagliai, and G. Cardini, "Absorption spectra of flexible fluorescent probes by a combined computational approach: Molecular dynamics simulations and time-dependent density functional theory," J. Phys. Chem. A **126**, 8809–8817 (2022).
[62]S. Matsuoka, T. Kohzuki, C. Pac, A. Ishida, S. Takamuku, M. Kusaba, N. Nakashima, and S. Yanagida, "Photocatalysis of oligo(p-phenylenes): Photochemical reduction of carbon dioxide with triethylamine," J. Phys. Chem. **96**, 4437–4442 (1992).
[63]H. Seo, M. H. Katcher, and T. F. Jamison, "Photoredox activation of carbon dioxide for amino acid synthesis in continuous flow," Nat. Chem. **9**, 453–456 (2017).
[64]H. Seo, A. Liu, and T. F. Jamison, "Direct β-selective hydrocarboxylation of styrenes with CO_2 enabled by continuous flow photoredox catalysis," J. Am. Chem. Soc. **139**, 13969–13972 (2017).
[65]E. Epifanovsky *et al.*, "Software for the frontiers of quantum chemistry: An overview of developments in the Q-Chem 5 package," J. Chem. Phys. **155**, 084801 (2021).
[66]A. Dreuw and M. Head-Gordon, "Single-reference ab initio methods for the calculation of excited states of large molecules," Chem. Rev. **105**, 4009–4037 (2005).
[67]J.-D. Chai and M. Head-Gordon, "Long-range corrected hybrid density functionals with damped atom–atom dispersion corrections," Phys. Chem. Chem. Phys. **10**, 6615–6620 (2008).
[68]J.-D. Chai and M. Head-Gordon, "Systematic optimization of long-range corrected hybrid density functionals," J. Chem. Phys. **128**, 084106 (2008).
[69]T. N. Truong and E. V. Stefanovich, "A new method for incorporating solvent effect into the classical, ab initio molecular orbital and density functional theory frameworks for arbitrary shape cavity," Chem. Phys. Lett. **240**, 253–260 (1995).
[70]V. Barone and M. Cossi, "Quantum calculation of molecular energies and energy gradients in solution by a conductor solvent model," J. Phys. Chem. A **102**, 1995–2001 (1998).
[71]M. Cossi, N. Rega, G. Scalmani, and V. Barone, "Energies, structures, and electronic properties of molecules in solution with the C-PCM solvation model," J. Comput. Chem. **24**, 669–681 (2003).
[72]J. Tomasi, B. Mennucci, and R. Cammi, "Quantum mechanical continuum solvation models," Chem. Rev. **105**, 2999–3094 (2005).
[73]Q. Ge and M. Head-Gordon, "Energy decomposition analysis for excimers using absolutely localized molecular orbitals within time-dependent density functional theory and configuration interaction with single excitations," J. Chem. Theory Comput. **14**, 5156–5168 (2018).
[74]R. Z. Khaliullin, E. A. Cobar, R. C. Lochan, A. T. Bell, and M. Head-Gordon, "Unravelling the origin of intermolecular interactions using absolutely localized molecular orbitals," J. Phys. Chem. A **111**, 8753–8765 (2007).
[75]R. M. Richard and J. M. Herbert, "Time-dependent density-functional description of the ^1L_a state in polycyclic aromatic hydrocarbons: Charge-transfer character in disguise?," J. Chem. Theory Comput. **7**, 1296–1306 (2011).
[76]I. Mayer, "Using singular value decomposition for a compact presentation and improved interpretation of the CIS wave functions," Chem. Phys. Lett. **437**, 284–286 (2007).
[77]P. R. Surján, "Natural orbitals in CIS and singular-value decomposition," Chem. Phys. Lett. **439**, 393–394 (2007).
[78]See http://iqmol.org for IQmol molecular viewer; accessed December 2022.
[79]See jmol.sourceforge.net/ for Jmol development team.
[80]R. Improta, V. Barone, G. Scalmani, and M. J. Frisch, "A state-specific polarizable continuum model time dependent density functional theory method for excited state calculations in solution," J. Chem. Phys. **125**, 054103 (2006).
[81]A. Jain, S. P. Ong, W. Chen, B. Medasani, X. Qu, M. Kocher, M. Brafman, G. Petretto, G.-M. Rignanese, G. Hautier, D. Gunter, and K. A. Persson, "FireWorks: A dynamic workflow system designed for high-throughput applications," Concurrency Comput.: Pract. Exper. **27**, 5037–5059 (2015).
[82]S. P. Ong, W. D. Richards, A. Jain, G. Hautier, M. Kocher, S. Cholia, D. Gunter, V. L. Chevrier, K. A. Persson, and G. Ceder, "Python materials genomics (pymatgen): A robust, open-source python library for materials analysis," Comput. Mater. Sci. **68**, 314–319 (2013).
[83]A. Behn, P. M. Zimmerman, A. T. Bell, and M. Head-Gordon, "Efficient exploration of reaction paths via a freezing string method," J. Chem. Phys. **135**, 224108 (2011).
[84]S. Mallikarjun Sharada, P. M. Zimmerman, A. T. Bell, and M. Head-Gordon, "Automated transition state searches without evaluating the Hessian," J. Chem. Theory Comput. **8**, 5166–5174 (2012).
[85]X.-H. Zhang, L.-Y. Wang, G.-H. Zhai, Z.-Y. Wen, and Z.-X. Zhang, "The absorption, emission spectra as well as ground and excited states calculations of some dimethine cyanine dyes," J. Mol. Struct.: THEOCHEM **906**, 50–55 (2009).
[86]A. Pedone, J. Bloino, S. Monti, G. Prampolini, and V. Barone, "Absorption and emission UV-Vis spectra of the TRITC fluorophore molecule in solution: A quantum mechanical study," Phys. Chem. Chem. Phys. **12**, 1000–1006 (2010).
[87]V. Barone, J. Bloino, S. Monti, A. Pedone, and G. Prampolini, "Fluorescence spectra of organic dyes in solution: A time dependent multilevel approach," Phys. Chem. Chem. Phys. **13**, 2160–2166 (2011).
[88]R. Królicki, W. Jarzęba, M. Mostafavi, and I. Lampre, "Preferential solvation of coumarin 153—The role of hydrogen bonding," J. Phys. Chem. A **106**, 1708–1713 (2002).
[89]A. V. Kityk, "Absorption and fluorescence spectra of heterocyclic isomers from long-range-corrected density functional theory in polarizable continuum approach," J. Phys. Chem. A **116**, 3048–3055 (2012).
[90]A. V. Marenich, C. J. Cramer, and D. G. Truhlar, "Universal solvation model based on solute electron density and on a continuum model of the solvent defined by the bulk dielectric constant and atomic surface tensions," J. Phys. Chem. B **113**, 6378–6396 (2009).
[91]A. Eilmes, "Solvatochromic probe in molecular solvents: Implicit versus explicit solvent model," Theor. Chem. Acc. **133**, 1538 (2014).
[92]L. Martínez-Fernández, A. J. Pepino, J. Segarra-Martí, A. Banyasz, M. Garavelli, and R. Improta, "Computing the absorption and emission spectra of 5-methylcytidine in different solvents: A test-case for different solvation models," J. Chem. Theory Comput. **12**, 4430–4439 (2016).
[93]T. Schwabe, J. M. H. Olsen, K. Sneskov, J. Kongsted, and O. Christiansen, "Solvation effects on electronic transitions: Exploring the performance of advanced solvent potentials in polarizable embedding calculations," J. Chem. Theory Comput. **7**, 2209–2217 (2011).